Topological Dirac states in asymmetric $Pb_{1-x}Sn_xTe$ quantum wells

M. A. Toloza Sandoval[a], G. C. La Rocca[b] and E. A. de Andrada e Silva[c]

[a]Instituto de Física, Universidade Federal da Bahia, 40210-340 Salvador, Bahia, Brazil
[b]Scuola Normale Superiore and CNISM, Piazza dei Cavalieri 7, I-56126 Pisa, Italy
[c]Instituto Nacional de Pesquisas Espaciais, C.P. 515, 12201-970 São José dos Campos, São Paulo, Brazil

ARTICLE INFO

Keywords:
Topological insulators
Lead-salt semiconductors
Spin-orbit coupling
Quantum wells

ABSTRACT

The electronic structure of lead-salt (IV-VI semiconductor) topological quantum wells (T-QWs) is investigated with analytical solutions of the effective 4x4 Dimmock $k \cdot p$ model, which gives an accurate description of the bands around the fundamental energy gap. Specific results for three-layer $Pb_{1-x}Sn_xTe$ nanostructures with varying Sn composition are presented and the main differences between topological and normal (N) QWs highlighted. A series of new features are found in the spectrum of T-QWs, in particular in asymmetric QWs where large (Rashba spin-orbit) splittings are obtained for the topological Dirac states inside the gap.

As in a normal $GaAs/AlGaAs$ quantum well (N-QW) carriers in topological quantum wells (T-QWs) are confined in a semiconducting nanolayer sandwiched by larger band-gap barrier materials. The difference is that in T-QWs the barriers or wells have inverted-gaps and the interfaces are between normal and topological insulators (TIs). The alignment of the bulk conduction and valence band edges in T and N-QWs are illustrated in Figure 1; there are also hybrid (H) QWs with one normal and one inverted-gap interface. N-QWs are at the basis of a whole chapter of both condensed matter physics and electronic device technology. It is likely that T-QWs will have a large impact too. However the features of this new class of semiconductor QWs that can be used in device applications [1, 2] are not yet fully understood.

The spin polarized electronic structure of symmetric and asymmetric IV-VI T-QWs is here studied with a realistic 4-band $k \cdot p$ model for the bulk and envelope-function approximation. The analytical and quantitative results obtained highlight the new features of T-QWs, extend previous theories and can be readily used for sample characterization and further studies of their electronic properties including the interface-bound metallic states which in 2D TIs as well as in the quantum Hall effect (QHE) are dissipation-less.

Historically in the 1980s, within newborn band-gap engineering, the spin-polarized states bound to inverted-gap interfaces (or surfaces) and laying inside the gap, were soon recognized in the envelope-function solutions for II-VI $HgCdTe$ [3, 4, 5, 6] , IV-VI $PbSnTe$ [7, 8, 6, 9] and III-V [10] narrow (or zero) gap semiconductor heterojunctions, surfaces and QWs, much like effective-mass domain walls. With high mobility III-V N-QWs, in the same period the QHE was discovered [11] and explained with the introduction of topological concepts [12]. Decades later the existence of TIs was understood [13, 14] and the interest in inverted-gap interfaces renewed. The low-energy states bound to such interfaces are now known to be robust (protected topologically) and 2D TIs have been realized in II-VI HgTe/CdTe [15, 16] and III-V InAs/GaSb [17] QWs in which a band crossing and corresponding topological to normal insulator (T-N) transition takes place as a function of the well width L. In parallel, completing the picture and motivated by the proposal of a spin-transistor [18], the physics of the Rashba (i.e. mesoscopic) spin-orbit (SO) interaction was developed [19, 20, 21, 22, 23]. The fundamental role of the SO interaction in the TI physics is well known, however, e.g., the Rashba splitting of the topological Dirac states in asymmetric T-QWs is not known yet.

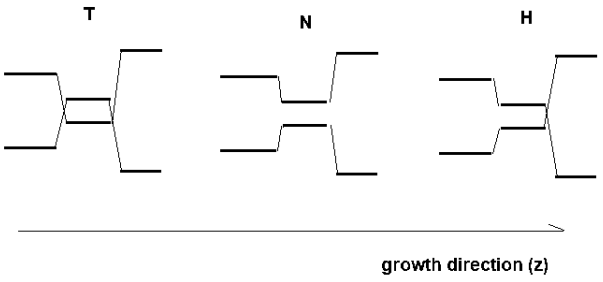

Figure 1: Conduction and valence bulk band edge alignment in topological (T), normal (N) and hybrid (H) semiconductor quantum wells.

Today the lead-salts, including in their family topological crystalline insulators (TCIs) [24] such as Sn rich $PbSnTe$ [25], form preferable topological structures in many respects [26, 27, 28, 29, 30, 31, 32]. With IV-VI 2D nanostructures [33] it is possible to fabricate simple T-QWs and study T-N transitions by varying composition, temperature or pressure. For example, at low temperatures by varying the Sn content x, the gap of $Pb_{1-x}Sn_xTe$ inverts at $x \simeq 0.4$ and the above three basic types of semiconductor QWs (T,N and H) can be easily grown with $Pb_{1-x}Sn_xTe$ three layer nanostructures with say x in the center (well), and x_1 and x_2 ($\neq x$) in the left and right layers (barriers) respectively. For instance, if $x \lesssim 0.4$ (i.e. on the $PbTe$ side of the gap-inversion) large x_1 and x_2 (i.e. Sn rich)

ORCID(s): 0000-0002-1071-6665 (M.A.T. Sandoval)

barriers give T-QWs, while Pb rich barriers give N-QWs, and vice-versa if $x \gtrsim 0.4$. In both cases, a Pb rich barrier on one side and a Sn rich on the other form H-QWs. Lead-salts are multi-valley semiconductors with four equivalent anisotropic valleys at the L-points of the Brillouin zone; and in a QW each non-equivalent valley leads to a different series of quantized states; the valleys (their main axis) will be either longitudinal or oblique (making an angle θ) to the growth direction. In [111] grown QWs one has one longitudinal and three oblique valleys, while in [100] grown QWs all four valleys are oblique.

It is known that in single inverted-gap interfaces (or in thick T-QWs, i.e with independent interfaces) exist inside the gap perfect Dirac cones of allowed states that are topological, spin-polarized, bound to the interface and metallic [7, 8, 6, 9]. As the well width of the thick T-QW is reduced, the states bound to the different interfaces start to interact and a gap is opened at the center of the cone [8, 26]. If the T-QW is symmetric, the states with opposite spins bound to opposite interfaces have the same energy and the spectra remains spin degenerate. Among the open questions there are: how the spin degeneracy is broken in asymmetric T-QWs (Rashba effect), including the resulting spin-texture; at what rate the gap of the Dirac cone increases with further decrease of L; how these effects vary between ground and excited states; and what is their quantitative dependence on valley type, growth direction and structure's parameters (i.e. bulk ones plus the band-offset) in realistic $PbSnTe$ T-QWs.

These questions are addressed here with (k-linear) Dimmock [34] 4-band $k \cdot p$ model which gives a very good description of the bulk electronic states around the fundamental gap (E_g) using as parameters the measured E_g and band-edge longitudinal and transverse effective masses m_l^* and m_t^*. The corresponding effective Hamiltonian for QW envelope-functions is solved analyticaly for the quantized energies from each non-equivalent valley in symmetric and asymmetric T, N and H-QWs, grown along the main crystallographic directions, i.e. [111] (valley main axis) and [100] (preferable cleavage). We note that in analogy with Dirac's equation, Dimmock's model can be projected into one of the bands (conduction or valence) and be written as a 2x2 k^2 (Schroedinger-like) effective Hamiltonian with explicit SO (Rashba) term [35, 36, 37, 38, 39]. The resulting Rashba coupling constant in this case is inversely proportional to E_g in contrast to the well known one for electrons in III-V QWs which is proportional (in first order) to the SO splitting in the valence band [23]. The 4x4 and 2x2 effective Hamiltonians are equivalent and give identical results; however, for the low-energy states inside the gap the use of the 4x4 effective Hamiltonian is clearly a more natural choice.

The Dimmock 4x4 effective Hamiltonianand is conveniently written as:

$$H = \begin{pmatrix} \Delta(z) + q(z) & \hat{O} \\ \hat{O} & -\Delta(z) + q(z) \end{pmatrix} \tag{1}$$

with

$$\hat{O} = P_l \hat{k}_{z'} \sigma_{z'} + P_t (\hat{k}_{y'} \sigma_{y'} + k_x \sigma_x), \tag{2}$$

where the diagonal elements are implicitly multiplied by I_{2x2}, $\hat{z}$ is parallel to the growth direction, $\Delta(z) = E_g(z)/2$ and $q(z)$, the band(gap-center)-offset, being step functions, with steps at the interfaces; $\hat{z}'$ the valley main-axis direction; P_l the longitudinal and P_t the transverse (to $\hat{z}'$) momentum matrix elements, determined by $P_{l,t}^2 = \hbar^2 E_g / 2m_{l,t}^*$, and with the ratio $r = P_t/P_l$ as a measure of the valley anisotropy; $\hat{x}$ ($= \hat{x}'$) is parallel to the interfaces, perpendicular to both $\hat{z}$ and $\hat{z}'$, and k_x a good quantum number. The valley (primed) and the structure (unprimed) coordinate systems are connected by a θ-rotation around $\hat{x}$, so that $z' = cos(\theta)z + sin(\theta)y$, and $y' = -sin(\theta)z + cos(\theta)y$ (see Fig. 2 right panel). Finally the σs are the Pauli spin matrices and $\hat{k}_\mu = -i\frac{d}{d\mu}$, $\mu = z', y'$.

This model has been used to calculate the electronic structure of different IV-VI nanostructures [40, 35, 41, 36, 37, 26, 38, 31], including topological superlattices [31] and quantum walls [26], in good agreement with the available experimental data. However, the studies of topological structures so far have concentrated mostly on the properties of the ground-state and longitudinal valley. Here we consider the general solution for the whole spectrum and investigate the electronic structure of all different types (N,T and H) of IV-VI QWs.

Following Ref. [8] it is convenient to begin with the spin-diagonalization of the Hamiltonian, i.e. to write

$$H = \begin{pmatrix} H_+ & 0 \\ 0 & H_- \end{pmatrix}$$

by using as base states the eigen-states of $\vec{\sigma}_0$ satisfying

$$\left[H, \begin{pmatrix} \vec{\sigma}_0 & 0 \\ 0 & -\vec{\sigma}_0 \end{pmatrix}\right] = 0\,; \tag{3}$$

which corresponds to $\vec{\sigma}_0 \hat{O} = -\hat{O}\vec{\sigma}_0$, and leads to

$$\vec{\sigma}_0 = \begin{pmatrix} \sigma_x & \sigma_y & \sigma_z \end{pmatrix} \begin{pmatrix} -k_y \\ (cos(\theta)^2 + r sin(\theta)^2) k_x \\ (r-1) cos(\theta) sin(\theta) k_x \end{pmatrix}. \tag{4}$$

This gives the spin-texture or momentum-spin locking illustrated in Figure 2 for both longitudinal and oblique valleys, where $\vec{\sigma}_0$ is shown as a function of the in-plane wave-vector. For the longitudinal ($\theta = 0$) valley as well as for spherical ($r = 1$) valleys, it is reduced to the well known $(-k_y, k_x, 0)$ helical and isotropic Rashba spin-texture. For oblique valleys with $r \neq 1$ the spin-texture is seen to be anisotropic with a non-zero out-of-the-plane (z) spin-component. Note that $\vec{\sigma}_0$ gives the direction of the (SO splitting) effective magnetic-field [22, 36, 37] and is independent of $\Delta(z)$ and of $q(z)$.

Next one then calculates the matrix elements of $H_\pm$. For the longitudinal valley the structure and valley coordinate

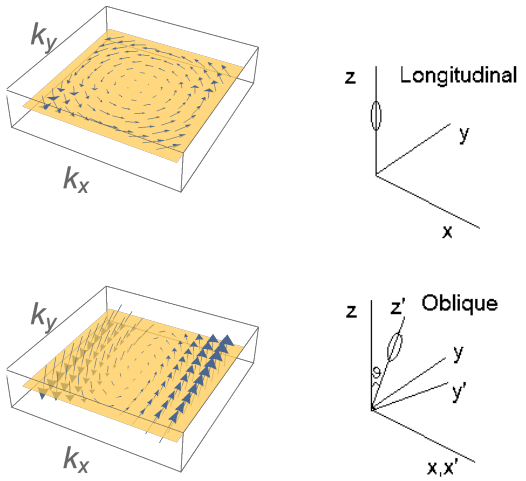

Figure 2: (color online) (Left) Spin-texture (or polarization) of the QW states derived from the longitudinal (top) and oblique (bottom) valleys, as a function of the in-plane wave-vector; (Right) Structure (unprimed) and valley (primed) coordinate systems.

systems coincide, there is rotation symmetry around $\hat{z}$ and the calculation is much simplified leading to:

$$H_{\pm} = H(\pm k) = \begin{pmatrix} \Delta + q & P_l\hat{k}_z \mp iP_tk \\ P_l\hat{k}_z \pm iP_tk & -\Delta + q \end{pmatrix} . \quad (5)$$

where $k = \sqrt{k_x^2 + k_y^2}$. For the oblique valleys one has to consider the coordinate transformation and resulting in-plane anisotropy. The calculation is much less straitforward, the expressions more complicated and we here discuss only the main results. In both cases though, the final solution for the QW states is then simply obtained by matching the bulk envelope-functions at each interface.

Recall that in the bulk $\Delta = E_g/2$ is constant, $q = 0$, the Hamiltonian has both space-inversion and electron-hole symmetries, and the specular symmetric spin-degenerate conduction and valence bands have the following relativistic dispersion relation

$$E_c = \sqrt{\Delta^2 + (P_lk_z)^2 + (P_tk)^2} \text{ and } E_v = -E_c , \quad (6)$$

and plane-wave envelope-functions of the form

$$\psi_{k_x,k_y,k_z}(z,\vec{r}_{\parallel}) = e^{i(k_xx+k_yy+k_zz)}\chi_{\pm};\ \chi_{\pm} = \begin{pmatrix} \frac{\Delta+E}{P_lk_z\pm iP_tk} \\ 1 \end{pmatrix} , \quad (7)$$

where $\pm$ is for the spin up and down, which are degenerate; for convenience the spin quantization direction is chosen along σ_0.

In heterostructures Δ varies along the growth direction ($\hat{z}$), P_l and P_t are assumed constants, the in-plane wave vector is conserved and the allowed energies are determined by the continuity of the envelope function at every interface, which assure continuity of the particle flux. For example, at an inverted-gap [111] interface at $z = 0$ (i.e with $\Delta = \Delta_0$ for $z < 0$ and $-\Delta_0$ for $z > 0$) in-gap evanescent waves $e^{\rho z}$ on the left and $e^{-\rho z}$ on the right ($\times e^{i(k_xx+k_yy)}$), where

$$\rho = \frac{1}{P_l}\sqrt{\Delta_0^2 + (P_tk)^2 - E^2} ,$$

can be matched and spin-polarized interface-bound states with $E = \pm P_tk$ are seen to be allowed (for the longitudinal valley and $q = 0$) forming the mentioned Dirac cone (of massless fermions). The result for a general [111] inverted-gap interface between materials 1 and 2 reads:

$$E_{\pm} = \frac{\Delta_1 q}{\Delta_1 + \Delta_2} \pm P_tk\sqrt{1 - (\frac{q}{\Delta_1 + \Delta_2})^2} , \quad (8)$$

where the origin of energy is set at the center of the gap on the left and the band-offset q gives the center of the gap on the right, and is seen to shift the energy position and slope of the cone.

For QWs, with just a little more algebra the allowed states are found from the continuity condition at both interfaces, e.g. $e^{+\rho_1 z}\chi_{\pm}^{(1)}(z) = (Ae^{+\rho z} + Be^{-\rho z})\chi_{\pm}$ at $z = -L/2$, and $(Ce^{+\rho z} + De^{-\rho z})\chi_{\pm} = e^{-\rho_2 z}\chi_{\pm}^{(2)}$ at $z = L/2$, for a QW centred at $z = 0$ with barrier materials 1 and 2 on the left and right, where

$$\rho_i = \frac{1}{P_l}\sqrt{\Delta_i^2 + (P_tk)^2 - (E - q_i)^2} ; \quad (9)$$

for the regular QW states (above the gap) $\rho \to ik_z$. Recall that for IV-VI nanostructures the neglect of band bendings (i.e. the use of flat bands) is a particularly good approximation in view of their large dielectric constants. As usual the QW solutions are not explicit as in the single interface case but obtained via a transcendental equation. For symmetrical T-QWs with material 1 on both sides the allowed quantized states are the solutions of:

$$[\Delta\Delta_1 + (E - q_1)E - P_t^2k^2]tanh(\rho L) = P_l^2\rho\rho_1 , \quad (10)$$

equation which for $q_1 = 0$ reduces to the one obtained by Korenman and Drew (Ref. [8] Eq. (5)). For N-QWs one simply changes the sign of Δ, and for H-QWs (with $q_1 = 0$) one obtains:

$$e^{2\rho L}[\Delta^2 + \Delta_1^2 + 2(P_t^2k^2 + P_l^2\rho\rho_1 - E^2)] = \Delta_1^2 - \Delta^2 . \quad (11)$$

Figure 3 shows specific results for the longitudinal valley electron states as a function of the well width of all kinds of $Pb_{0.7}Sn_{0.3}Te$ [111] QWs at low temperatures with $E_g^w(= 2\Delta) = 40\ meV$, and $Pb_{1-x_1}Sn_{x_1}Te$ barriers with $E_g^b(= 2\Delta_1) = 190\ meV$, corresponding to $x_1 = 0$ (i.e. pure $PbTe$)

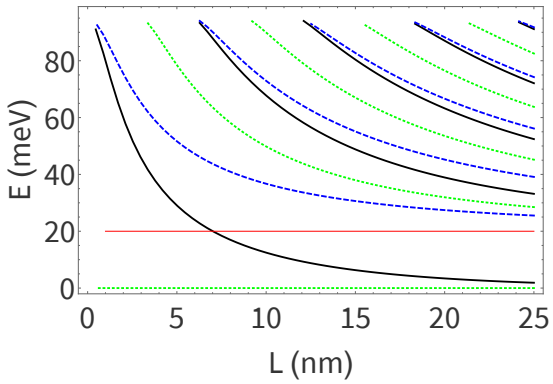

Figure 3: (color online) Quantized energy levels of Topological $Pb_{0.2}Sn_{0.8}Te/Pb_{0.7}Sn_{0.3}Te/Pb_{0.2}Sn_{0.8}Te$ (black continuous lines), Normal $PbTe/Pb_{0.7}Sn_{0.3}Te/PbTe$ (blue dashed lines) and Hybrid $PbTe/Pb_{0.7}Sn_{0.3}Te/Pb_{0.2}Sn_{0.8}Te$ (green dotted lines) symmetric QWs, all with $E_g^b = 190$ and $E_g^w = 40\ meV$. The bulk band edge (or gap) is signed with the thin (red) line and for the hole states note that the spectrum is specular with respect to $E = 0$ (mid-gap) due to the e-h symmetry. The parameters used are the low-temperature $PbTe$ effective mass $m_l^* = 0.24\, m_e$ and $m_t^* = 0.024\, m_e$ and $Pb_{1-x}Sn_xTe$ gap $E_g(x) = 0.19 - 0.48\, x\ eV$.

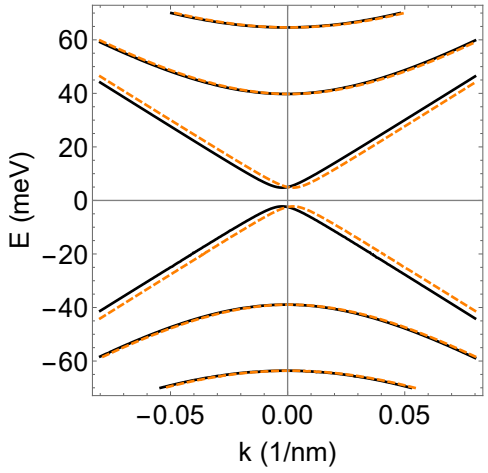

Figure 4: (color online) Spin-split electron and hole subbands in asymmetric $Pb_{0.2}Sn_{0.8}Te/Pb_{0.7}Sn_{0.3}Te/SnTe$ T-QW, with $L = 20\ nm$ and a band-offset $q = 20\ meV$.

in the case of N-QWs and $x_1 = 0.8$ in that of T-QWs. The states for holes are obtained with a specular reflection at $E = 0$ and it is assumed $q_1 = 0$. As expected, due to the confinement, the subband-edge energies (i.e., for $k = 0$) shown increase with decreasing L in all three types. The main difference is that T and H QWs allow for states inside the gap (i.e. with $E < 20\ meV$). For T-QWs these states are spin degenerate and the observed energy increase for decreasing L corresponds to the gap openning at the Dirac cone center, and is due to hybridization between the states bound to opposed interfaces. For H-QWs on the other hand these interface states are spin-polarized, pinned to zero and bound to the inverted-gap one. It is also interesting to note

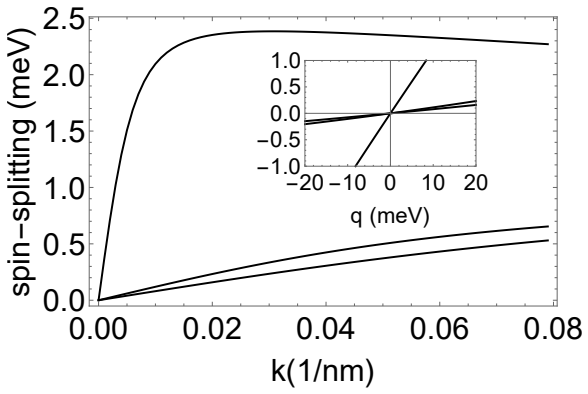

Figure 5: Electron subbands spin-splitting of the $L = 20\ nm$ T-QW of Figure 4, as a function of the parallel wave-vector k. The inset shows the dependence on band off-set q for a fixed k ($= 0.02\ nm^{-1}$).

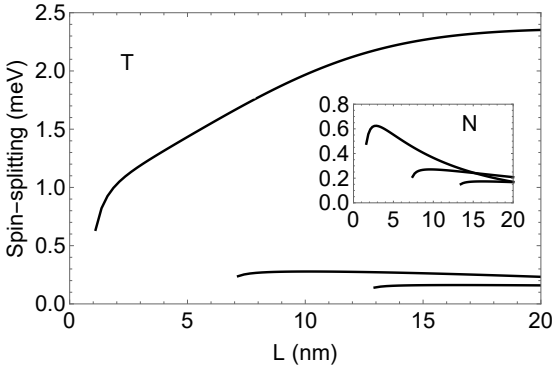

Figure 6: Spin-splittings of the subbands at $k = 0.02\ nm^{-1}$ for $PbSnTe$ T-QWs (as in Figure 4) with varying well width L. In the inset, the corresponding results for N-QWs.

that at higher energies the spectra of T and N-QWs tend to be similar as the nature of the gap in the well (i.e. if inverted or not) gets less important, and that the levels of the H-QWs lay right in between those of the N-QWs (or T-QWs).

The differences though are bigger and more interesting for spintronics applications in the case of asymmetric QWs. As in the better known (III-V) Rashba effect, the SO splitting of the electron and hole subbands in IV-VI T-QWs requires structure inversion asymmetry (SIA). However, in their case due to electron-hole symmetry, $\Delta(z) \neq \Delta(-z)$ is not sufficient; $q \neq 0$ in at least one of the two interfaces to break the e-h symmetry is necessary. As an example, in Figure 4 it is shown the obtained dispersion relations for the (isotropic longitudinal) electron and hole subbands of a $Pb_{0.2}Sn_{0.8}Te/Pb_{0.7}Sn_{0.3}Te/SnTe$ asymmetric T-QW, with $L = 20\ nm$. The band-offset between $Pb_{1-x}Sn_xTe$ and $SnTe$ is not well known and in the figure a $q_2 = 20\ meV$ is used ($q_1 = 0$). Continuous and dashed lines give

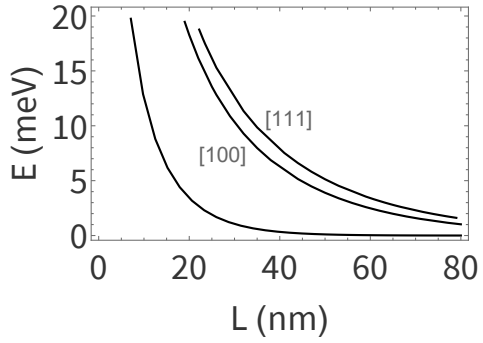

Figure 7: Comparison between the interfaces states deriving from longitudinal and oblique valleys, the last one both for [100] and [111] $PbSnTe$ T-QWs ($E_g^b = 190$ and $E_g^w = 40$ meV).

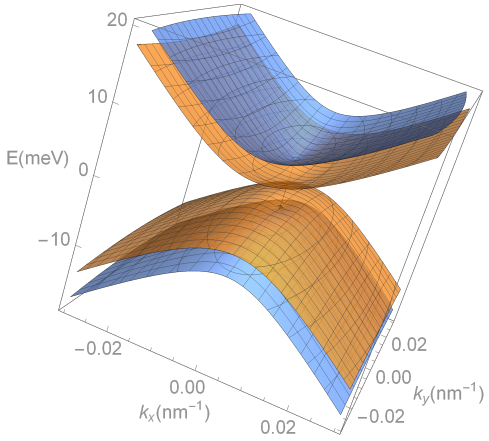

Figure 8: (color online) Anisotropic and gapped Dirac cone of interface states from the oblique valleys in a [111] ($L = 60$ nm) T-QWs.

the Rashba SO split dispersion relations for both electron and hole subbands, obtained as the solutions of the following equation which generalizes Eq.(10) to the asymmetric QW case:

$$\Big\{(\Delta+E)P_l^2\rho_1\rho_2 - P_t^2k^2(\Delta_1'+\Delta_2'+\Delta-E) - E^3$$
$$+E^2(\Delta_1'+\Delta_2'+\Delta) - E\Delta(\Delta_1'+\Delta_2') + (\Delta-E)\Delta_1'\Delta_2'$$
$$\pm P_lP_tk\left[(\Delta_1'+\Delta)\rho_2 - (\Delta_2'+\Delta)\rho_1\right]\Big\}tanh(\rho L)$$
$$= P_l^2\left[(\Delta_1'-E)\rho\rho_2 + (\Delta_2'-E)\rho\rho_1\right] \mp P_lP_t\rho k(\Delta_1'-\Delta_2'), \quad (12)$$

where $\Delta_i' = \Delta_i + q_i$, $i = 1, 2$. The spin-splitting as a function of the parallel wave-vector k and its dependence on the band-offset q are plotted in Figure 5 for both interface-bound and above the gap (regular) QW subbands, where it is noted that while for the regular subbands the splitting increases as expected linearly with k (with a slowly decreasing slope), that for the interface-bound states instead, besides being one order of magnitude larger, is seen to initialy increase very fast with k and then to present a maximum. For a fixed k ($= 0.02$ nm^{-1}) the inset shows the splitting sign change and linear variation with q. Figure 6 compares the well-width dependence of the splitting in T and similar N-QWs (inset), and shows different behaviours in particular conserning the T-QW interface bound states which are seen to present decreasing spin-splittings with decreasing L. It is known that such SO splitting is determined both by the amplitudes of the envelope-functions at the interfaces and by the energy dependent coupling parameter; such increase with L for the in-gap states for instance derives from the increasing coupling with the decreasing gap (in the Dirac cone).

The $E_{l,n}$ series of quantized states derived from the longitudinal valley in T-QWs discussed so far give the simplest example of the T-QW new features and the ground state of [111] QWs. To complete the spectra of the [111] QW and to calculate that for [100] QWs, we now discuss the results for the oblique valleys which mainly introduce in-plane anisotropy in the dispersion relations. For example in a single inverted-gap interface (or thick T-QW) the

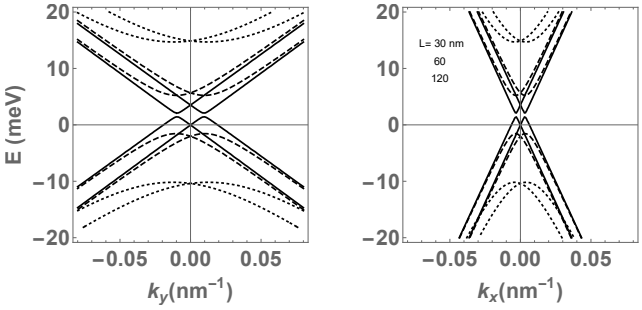

Figure 9: Dispersion relation for the spin split interface-bound states derived from the oblique valleys in [111] asymmetric T-QWs with $L = 120, 60$ and 30 nm, and $q_1 = 0, q_2 = 20$ meV, $\Delta_1 = 95, \Delta_2 = 95$ meV, for wave-vectors along $\hat{x}$ and $\hat{y}$.

dispersion relation of the (interface-bound) allowed states from the oblique valleys satisfy the same Eq.(8) above with k substituted by $\sqrt{k_x^2 + (\frac{9}{1+8r^2})k_y^2}$ for [111] QWs and by $\sqrt{k_x^2 + (\frac{3}{1+2r^2})k_y^2}$ for [100] QWs, describing elliptical Dirac cones.

The subbands derived from the oblique valleys in [111] T-QWs are higher in energy but with similar properties as the longitudinal ones. Figure 7 gives specific results for the oblique-valley subband edge dependence on L and on the growth direction, compared with the [111] ground state (longitudinal) for the same QW structure of Fig. 3. It is observed that the gap at the center of the (ellipitical) Dirac cones of interface states from the oblique valleys opens much faster than that for the longitudinal valley as the QW width is reduced (recall that in the figure only half of the gap is seen as the hole states are given by the specular reflection at $E = 0$) so that for thin wells the QW low energy states are all longitudinal. In Figure 8 typical results for the Rashba split gapped elliptical cones of interface-bound states derived from the oblique valleys in a [111] ($L = 60\,nm$) asymmetric $PbSnTe$ T-QW are shown. The obtained spin-splitting and

well-width dependence are presented in Figure 9 where the dispersion relations of Fig. 8 are plotted for wave-vectors along $\hat{y}$ and $\hat{x}$, compared with the results for QWs with well-width twice as large and twice as smaller, and seen to present the expected gap opening with decreasing L and typical Rashba SO splittings, except for the inplane anisotropy and the massless dispersions for large L and small gap.

In conclusion we have discussed the theory of the electronic structure of IV-VI semiconductor topological QWs and its new features with respect to the well known GaAs-like normal QWs. Within envelope-function and four-band $k \cdot p$ approximations, analytical expressions were obtained that give the energy spectra of this new class of semiconductor QWs, including the new and technological spin-polarized Dirac states bound to the inverted-gap interfaces. With specific and quantitative results for simple three layer $Pb_{1-x}Sn_xTe$ T-QWs, the effects of varying well-width, growth direction, band-offset, valley type and that of spin-orbit splitting in asymmetric QWs were shown. Detailed results for the spin splitting of such in-gap states in asymmetric IV-VI T-QWs demostrate different behavious compared to the better known III-V Rashba effect besides values near one-order of magnitude larger. The theory and specific results presented are bound to help the development and fabrication of new electronic devices using IV-VI T-QWs.

Acknowledgments: EAAS is thankful to FAPESP Brazil (2016/03854-9) and to Scuola Normale Superiore di Pisa for the support. This study also was financed in part by the Coordenação de Aperfeiçoamento de Pessoal de Nível Superior - Brazil (CAPES) - PNPD 88882.306206/2018-01.

References

[1] C. Yue, S. Jiang, H. Zhu, L. Chen, Q. Sun, D. W. Zhang, Device applications of synthetic topological insulator nanostructures, Electronics 7 (2018) 225.

[2] A. Zhang, F. Wei, C. Yan, F. Wang, S. Ma, Z. Zhang, Topological phase transition and highly tunable topological transport in topological crystalline insulator $Pb_{1-x}Sn_xTe$ (111) thin films, Nanotechnology 30 (2019) 275703.

[3] M. I. D'Yakonov, A. V. Khaetskiĭ, Surface states in a gapless semiconductor, ZhETF Pisma Redaktsiiu 33 (1981) 115.

[4] Y. R. Lin-Liu, L. J. Sham, Interface states and subbands in HgTe-CdTe heterostructures, Phys. Rev. B 32 (1985) 5561–5563.

[5] N. A. Cade, Quantum well bound states of HgTe in CdTe, Journal of Physics C: Solid State Physics 18 (1985) 5135–5141.

[6] O. Pankratov, S. Pakhomov, B. Volkov, Supersymmetry in heterojunctions: Band-inverting contact on the basis of $Pb_{1-x}Sn_xTe$ and $Hg_{1-x}Cd_xTe$, Solid State Communications 61 (1987) 93 – 96.

[7] B. Volkov, O. Pankratov, JETP Letters 42 (1985) 178.

[8] V. Korenman, H. D. Drew, Subbands in the gap in inverted-band semiconductor quantum wells, Phys. Rev. B 35 (1987) 6446–6449.

[9] D. Agassi, V. Korenman, Interface states in band-inverted semiconductor heterojunctions, Phys. Rev. B 37 (1988) 10095–10106.

[10] R. A. Suris, Surface states in heterojunction, Sov. Phys. Semicond. 20 (1986) 1258.

[11] K. v. Klitzing, G. Dorda, M. Pepper, New method for high-accuracy determination of the fine-structure constant based on quantized Hall resistance, Phys. Rev. Lett. 45 (1980) 494–497.

[12] D. J. Thouless, M. Kohmoto, M. P. Nightingale, M. den Nijs, Quantized Hall conductance in a two-dimensional periodic potential, Phys. Rev. Lett. 49 (1982) 405–408.

[13] M. Z. Hasan, C. L. Kane, Topological insulators, Rev. Mod. Phys. 82 (2010) 3045–3067.

[14] X.-L. Qi, S.-C. Zhang, Topological insulators and superconductors, Rev. Mod. Phys. 83 (2011) 1057–1110.

[15] B. A. Bernevig, T. L. Hughes, S.-C. Zhang, Quantum spin Hall effect and topological phase transition in HgTe quantum wells, Science 314 (2006) 1757–1761.

[16] M. König, S. Wiedmann, C. Brüne, A. Roth, H. Buhmann, L. W. Molenkamp, X.-L. Qi, S.-C. Zhang, Quantum spin Hall insulator state in HgTe quantum wells, Science 318 (2007) 766–770.

[17] I. Knez, R.-R. Du, G. Sullivan, Evidence for helical edge modes in inverted InAs/GaSb quantum wells, Phys. Rev. Lett. 107 (2011) 136603.

[18] S. Datta, B. Das, Electronic analog of the electro-optic modulator, Applied Physics Letters 56 (1990) 665–667.

[19] J. P. Eisenstein, H. L. Störmer, V. Narayanamurti, A. C. Gossard, W. Wiegmann, Effect of inversion symmetry on the band structure of semiconductor heterostructures, Phys. Rev. Lett. 53 (1984) 2579–2582.

[20] G. Lommer, F. Malcher, U. Rossler, Spin splitting in semiconductor heterostructures for B going to 0, Phys. Rev. Lett. 60 (1988) 728–731.

[21] J. Luo, H. Munekata, F. F. Fang, P. J. Stiles, Effects of inversion asymmetry on electron energy band structures in GaSb/InAs/GaSb quantum wells, Phys. Rev. B 41 (1990) 7685–7693.

[22] E. A. de Andrada e Silva, Conduction-subband anisotropic spin splitting in III-V semiconductor heterojunctions, Phys. Rev. B 46 (1992) 1921–1924.

[23] E. A. de Andrada e Silva, G. C. La Rocca, F. Bassani, Spin-split subbands and magneto-oscillations in III-V asymmetric heterostructures, Phys. Rev. B 50 (1994) 8523–8533.

[24] L. Fu, Topological crystalline insulators, Phys. Rev. Lett. 106 (2011) 106802.

[25] S.-Y. Xu *et al.*, Observation of a topological crystalline insulator phase and topological phase transition in $Pb_{1-x}Sn_xTe$, Nature Communications 3 (2012) 1192.

[26] R. Buczko, L. Cywiński, PbTe/PbSnTe heterostructures as analogs of topological insulators, Phys. Rev. B 85 (2012) 205319.

[27] S. Safaei, P. Kacman, R. Buczko, Topological crystalline insulator (Pb, Sn)Te: Surface states and their spin polarization, Phys. Rev. B 88 (2013) 045305.

[28] G. Yang, J. Liu, L. Fu, W. Duan, C. Liu, Weak topological insulators in PbTe/SnTe superlattices, Phys. Rev. B 89 (2014) 085312.

[29] T. Liang, S. Kushwaha, J. Kim, Q. Gibson, J. Lin, N. Kioussis, R. J. Cava, N. P. Ong, A pressure-induced topological phase with large berry curvature in $Pb_{1-x}Sn_xTe$, Science Advances 3 (2017).

[30] A. Łusakowski, P. Bogusławski, T. Story, Alloy broadening of the transition to the nontrivial topological phase of $Pb_{1-x}Sn_xTe$, Phys. Rev. B 98 (2018) 125203.

[31] G. Krizman, B. A. Assaf, T. Phuphachong, G. Bauer, G. Springholz, G. Bastard, R. Ferreira, L. A. de Vaulchier, Y. Guldner, Tunable dirac interface states in topological superlattices, Phys. Rev. B 98 (2018) 075303.

[32] S. Kalish, C. Chamon, M. El-Batanouny, L. H. Santos, R. Sankar, F. C. Chou, Contrasting the surface phonon dispersion of $Pb_{0.7}Sn_{0.3}Se$ in its topologically trivial and nontrivial phases, Phys. Rev. Lett. 122 (2019) 116101.

[33] G. Springholz, G. Bauer, Molecular beam epitaxy of IV-VI semiconductor hetero- and nano-structures, phys. stat. sol. (b) 244 (2007) 2752–2767.

[34] J. O. Dimmock, in *The Physics of Semimetals and Narrow-Gap Semiconductors*, Edited by D. L. Carter and R.T. Bate (Pergamon, Oxford) (1971).

[35] E. A. de Andrada e Silva, Optical transition energies for lead-salt semiconductor quantum wells, Physical Review B 60 (1999) 8859.

[36] M. M. Hasegawa, E. A. de Andrada e Silva, Spin-orbit-split subbands in IV-VI asymmetric quantum wells, Physical Review B 68 (2003) 205309. (note the misprints in the equations (8) and (9), on the right the wave-vector components should be squared, and (11) where it

should be q instead of k).

[37] M. M. Hasegawa, E. A. de Andrada e Silva, G. C. L. Rocca, Electron-hole symmetry and spin-orbit splitting in IV-VI asymmetric quantum wells, Physica E: Low-dimensional Systems and Nanostructures 20 (2004) 400–403.

[38] E. Ridolfi, E. A. de Andrada e Silva, G. C. La Rocca, Effective g-factor tensor for carriers in IV-VI semiconductor quantum wells, Phys. Rev. B 91 (2015) 085313.

[39] V. I. Litvinov, Zero-field spin splitting in topological quantum wells, Phys. Rev. B 97 (2018) 235438.

[40] M. Kriechbaum, K. E. Ambrosch, E. J. Fantner, H. Clemens, G. Bauer, Phys. Rev. B 30 (1984) 3394–3405.

[41] E. Abramof, E. A. de Andrada e Silva, S. Ferreira, P. Motisuke, P. Rappl, A. Ueta, Optical spectra of PbTe/$Pb_{1-x}Eu_x$Te quantum wells, Physical Review B 63 (2001) 085304.